Supplementary Information

Polyoxometalate-cyclodextrin aggregates in isolation: Probing the conformer space and binding affinities

Papri Chakraborty,[1,2]* Manuel Link,[3] Christoph Plett,[4] Marco Neumaier,[2] Patrick Weis,[3] Masooma Ibrahim,[2] Stefan Grimme,[4]* and Manfred M. Kappes[2,3]*

[1]Institute for Quantum Materials and Technologies, Karlsruhe Institute of Technology, Kaiserstraße 12, 76131 Karlsruhe, Germany

[2]Institute of Nanotechnology, Karlsruhe Institute of Technology, Kaiserstraße 12, 76131 Karlsruhe, Germany

[3]Institute of Physical Chemistry, Karlsruhe Institute of Technology, Kaiserstraße 12, 76131 Karlsruhe, Germany

[4]Mulliken Center for Theoretical Chemistry, Universität Bonn, Beringstraße 4, 53115 Bonn, Germany

Table of Contents

List of Figures

List of Tables

Materials

All chemicals were purchased from VWR Chemicals and used without further purification. The following reagents were used for the synthesis of the Wells Dawson polyoxometalate $K_6[P_2W_{18}O_{62}]\cdot 14H_2O$: sodium tungstate dihydrate ($Na_2WO_4\cdot 2H_2O$, ≥99%), hydrochloric acid (HCl, 37%), phosphoric acid (H_3PO_4, 85%), and potassium chloride (KCl, ≥99.5%). Distilled water was used throughout the synthesis.

Methods

1. Photoelectron spectroscopy (PES)

PES spectra were taken using a previously reported machine.[1] A new laser system by EKSPLA (NT342 Series, 20 Hz pulse frequency, ns pulses) has been introduced to the instrument. It utilizes an OPO to generate wavelengths between 210 nm and 2000 nm. For the PES measurements, mass selected ion packets were perpendicularly hit by the laser beam. Photodetached electrons are guided by a magnetic field through a magnetic bottle type TOF-spectrometer perpendicular to the ion path and the laser beam. The electron signal is detected by a stack of MCPs. The signal is then processed by a preamplifier and digitized with a multichannel scaler (Type 7888-2) by Fast Comtec with a bin size of 1 ns. Background correction is done by alternating between measurements with and without ions present in the detachment region (40 s: 20 s split). The resulting TOF-spectrum is converted to a kinetic energy spectrum via calibration with $IrBr_6^{2-}$.[2]

The kinetic energy of electrons (EKE) can be transformed to their electron binding energy (EBE) using the expression, $EBE = h\nu - \mathrm{EK}E$. The energy spectrum consists of transitions to the different vibrational states of the species (multianion) with one electron less. Such transitions are too close in energy to be distinguished and are seen as their envelope instead.

PES spectra are used to obtain adiabatic detachment energies (ADEs, vibrational ground state transition), vertical detachment energies (VDEs, most probable transition) and repulsive Coulomb barriers (RCBs). RCBs are the barriers caused by the ion charge that electrons have to overcome in multianions (that retain a charge after electron detachment). They reflect both a short-range electron binding force and long-range coulomb repulsion between the outgoing photo-detached electron and resulting anion. RCBs prevent detachment of photoelectrons of higher BEs (corresponding to lower electron KEs). They result in a characteristic cutoff on the higher EBE side of the PES spectrum. The magnitude of RCB can be estimated from the difference of the incident photon energy and this spectral cutoff at the higher EBE side.

ADEs correspond to the threshold (rising flank on the lower EBE side) and VDEs correspond to the maximum of the first electron loss peak in the EBE spectrum. Measured ADEs can be used to determine the stabilization of the anions caused by the addition of γ-CD.

VDEs can only be determined if the electron peak is not cut off by the repulsive Coulomb barrier. This can be determined only by measuring the spectrum at additional detachment wavelengths. RCBs on the other hand can only be measured if a cut off is present in the spectrum. This, again, can only be verified by looking at different excitation wavelengths.

In exceptional cases (as perhaps occurring here for $[KPOM]^{5-}$) laser excitation may also lead to efficient excited state electron tunneling detachment (ESETD). This is associated with a constant EKE feature in the corresponding PE spectra independent of detachment wavelength. ESETD can make RCB assignment problematic. A rule of thumb for such cases is that RCB > EKE (ESETD). In the absence of systematic measurements at additional detachment wavelengths to more cleanly differentiate ESETD contributions from the PE spectra we presently locate RCB ≥ 4 eV for $[KPOM]^{5-}$.

2. Autodetachment measurements

The autodetachment measurements of $[HPOM]^{5-}$ were performed on a Thermo Scientific LTQ Orbitrap XL instrument, equipped with an electrospray source. First, $[HPOM]^{5-}$ (m/z = 873) was isolated in the linear ion trap of the instrument with an isolation width 10. By this, all other ion species were removed from the trap. In a second step $[HPOM]^{5-}$ was stored for a variable "activation" time (up to 50 s) with ion activation turned off (NCE=0). The emerging $[HPOM]^{4-}$ signal (m/z=1091) was detected as function of time in the orbitrap detector of the instrument. This was the only product ion channel. The complete isotope distributions were integrated. Finally, the relative intensity of $[HPOM]^{4-}$ was obtained by normalizing against the total ($[HPOM]^{4-}$ and $[HPOM]^{5-}$) ion intensities and correcting for their different charge states because of the charge sensitive detection in the orbitrap detector, i.e. $I_{rel}([HPOM]^{4-}) = I([HPOM]^{4-})/(I([HPOM]^{5-})\cdot 0.8+I([HPOM]^{4-}))$.

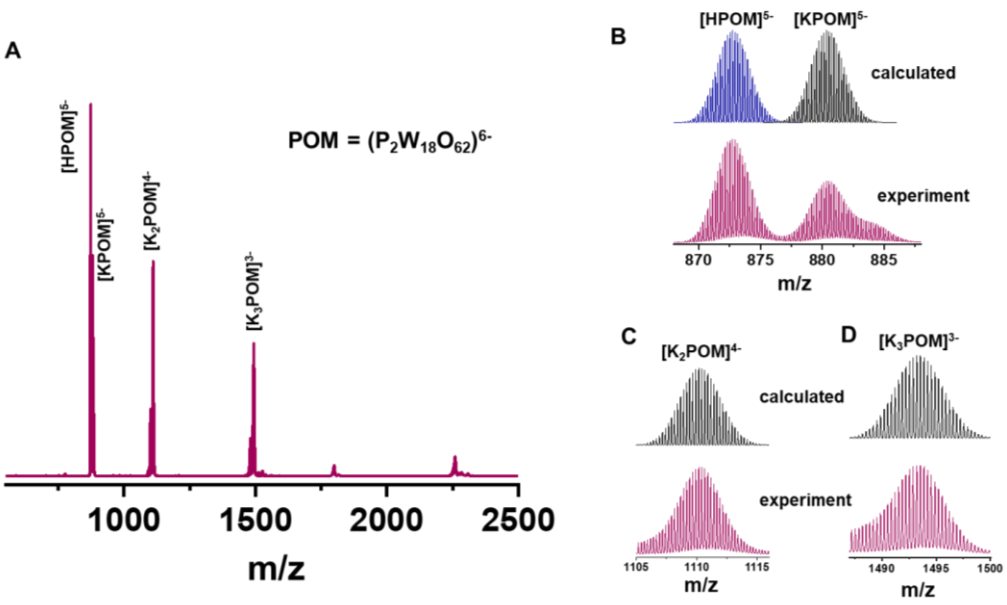

Fig. S1 A) ESI MS of POM, ionized in multiple charge states depending on the number of K^+ ions attached, Comparison of experimental and calculated isotopic patterns of B) $[HPOM]^{5-}$ and $[KPOM]^{5-}$, C) $[K_2POM]^{4-}$ and D) $[K_3POM]^{3-}$.

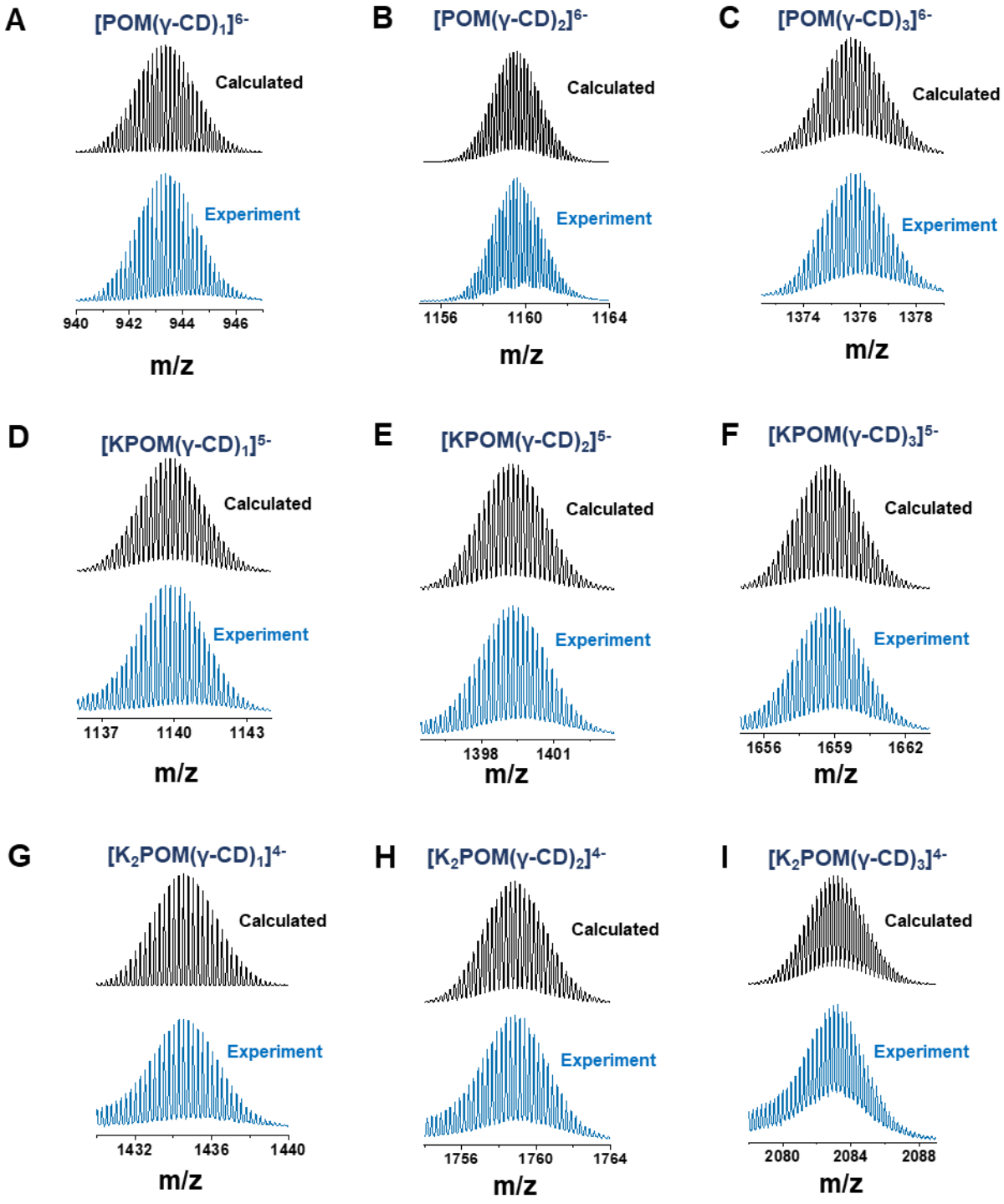

Fig. S2 Comparison of experimental and calculated isotopic patterns of the peaks $[K_xPOM(\gamma\text{-}CD)_n]^{(6-x)-}$ (x=0-2, n=1-3).

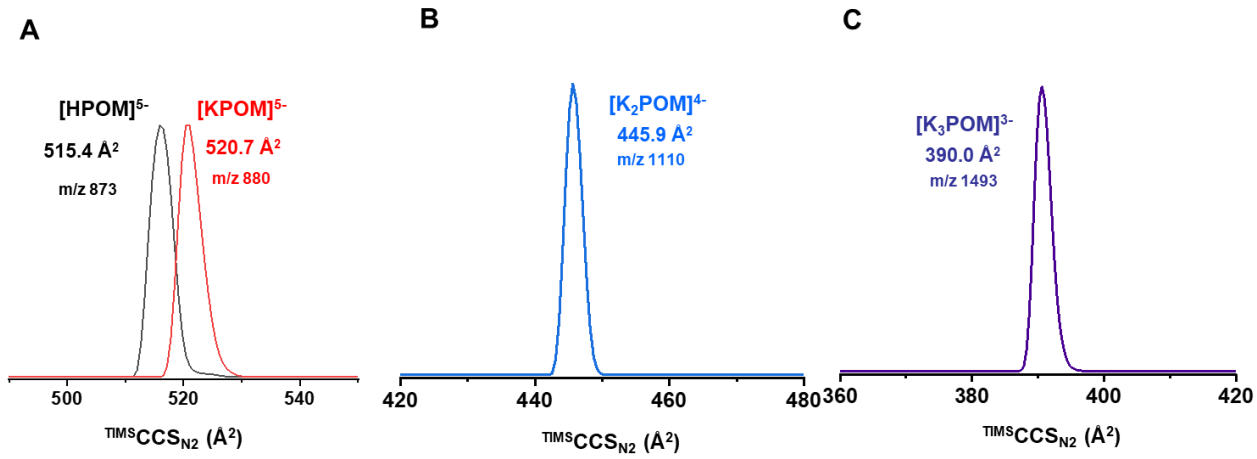

Fig. S3 TIMS spectra of A) $[HPOM]^{5-}$ and $[KPOM]^{5-}$, B) $[K_2POM]^{4-}$ and C) $[K_3POM]^{3-}$. $^{TIMS}CCS_{N2}$ denoted here are the mean values with standard error ≤ 0.5 Å^2.

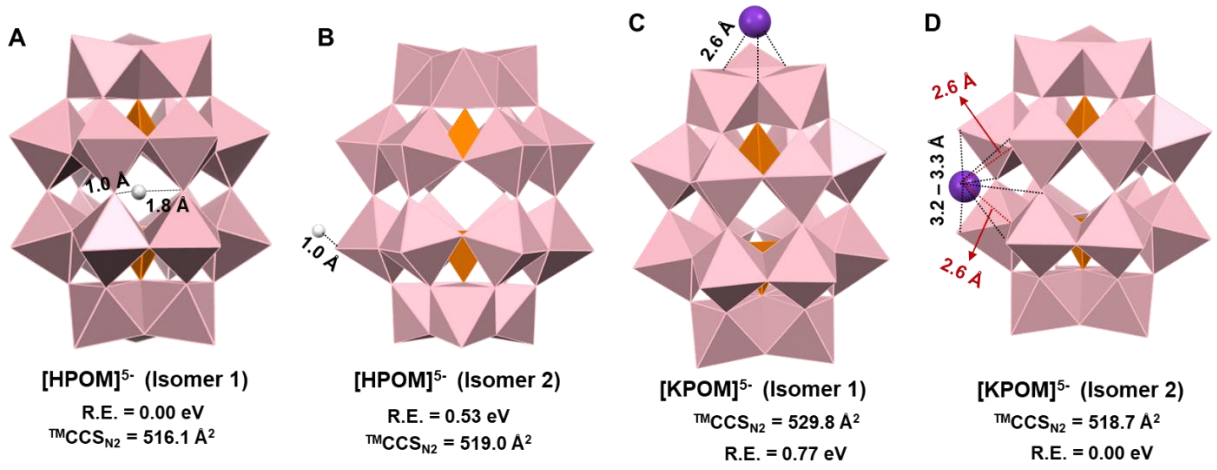

Fig. S4 DFT optimized structures of A), B) isomeric structures of $[HPOM]^{5-}$ and B, C) Isomeric structures of $[KPOM]^{5-}$.

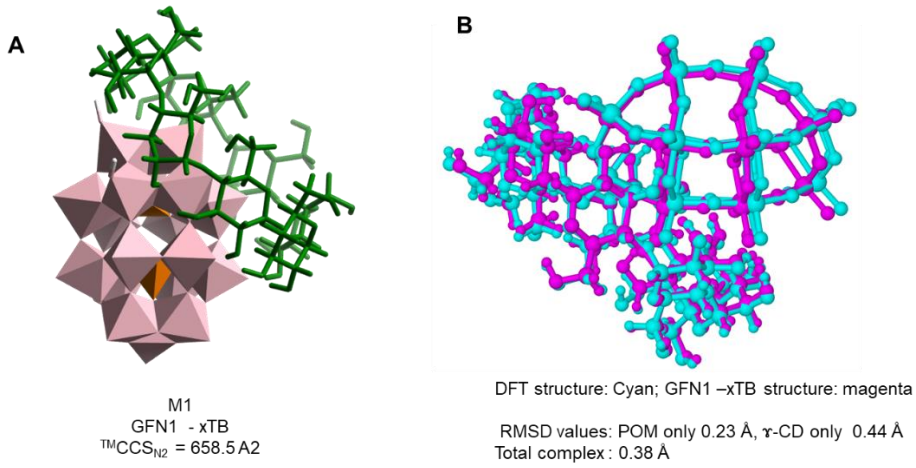

Fig. S5 A) Structure of M1 ($[POM(\gamma\text{-}CD)_1]^{6-}$), optimized by GFN1-xTB method and B) comparison of structure M1, optimized by DFT and xTB methods. Color codes in A: pink: WO_6 octahedron, orange: PO_4 tetrahedron, γ-CDs is colored in green, white: H transferred to POM surface from γ-CD during xTB optimization.

Note: In Fig. S4, we found that protonation on bridging oxo group (W-O-W) (Isomer 1) is more favorable than that on terminal oxo (W=O) group (Isomer 2). Here, GFN1-xTB optimization showed protonation on terminal oxo group for structure M1. However, DFT optimization of M1 did not show any proton transfer. The proton transfer observed here is likely an artifact of the xTB process.

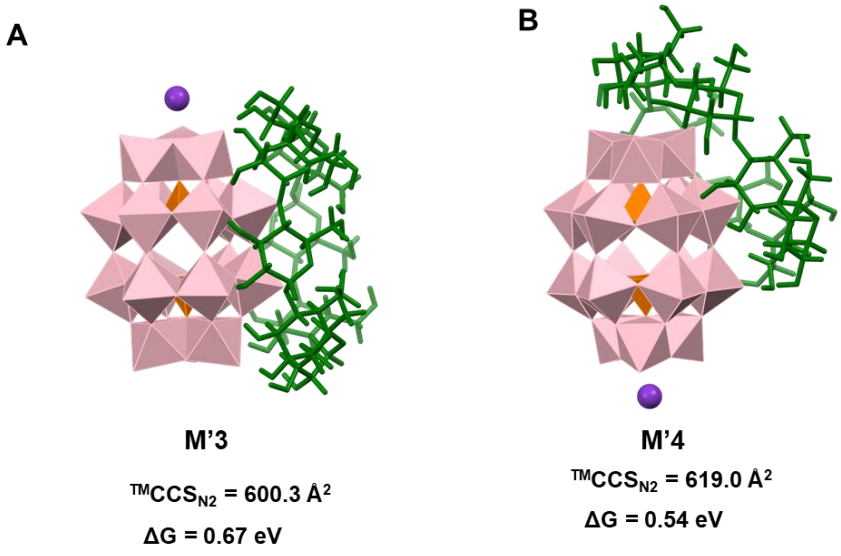

Fig. S6 DFT optimized structures of $[KPOM]^{5-}$ isomers M′3 and M′4. ΔG is the relative free energy, computed using wB97X-V method. The standard error in the mean $^{TM}CCS_{N2}$ values denoted here is <0.4%.

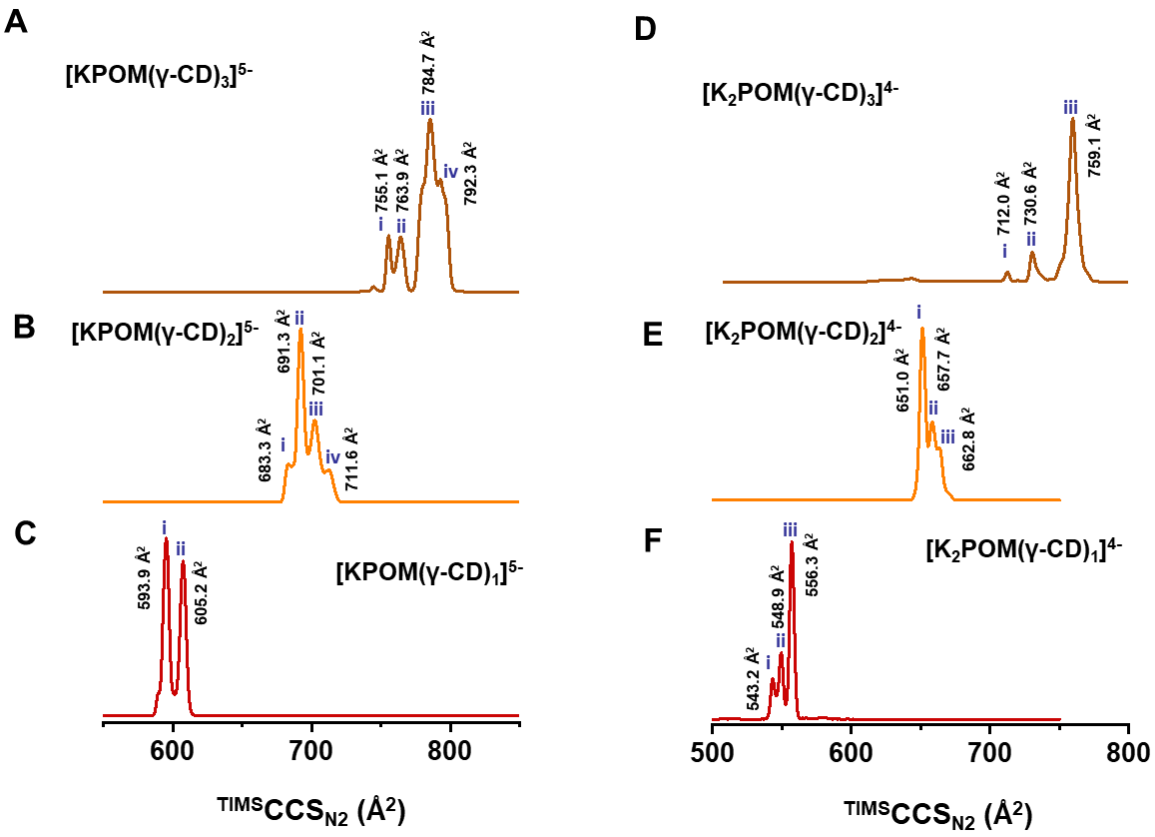

Fig. S7 TIMS spectra of A-C) $[KPOM(\gamma\text{-}CD)_n]^{5-}$ (n=1-3) and D-F) $[K_2POM(\gamma\text{-}CD)_n]^{4-}$ (n=1-3).The mean values of $^{TIMS}CCS_{N2}$ based on three different measurements is denoted here and the standard error for these species was < 1.5 Å^2 in all cases.

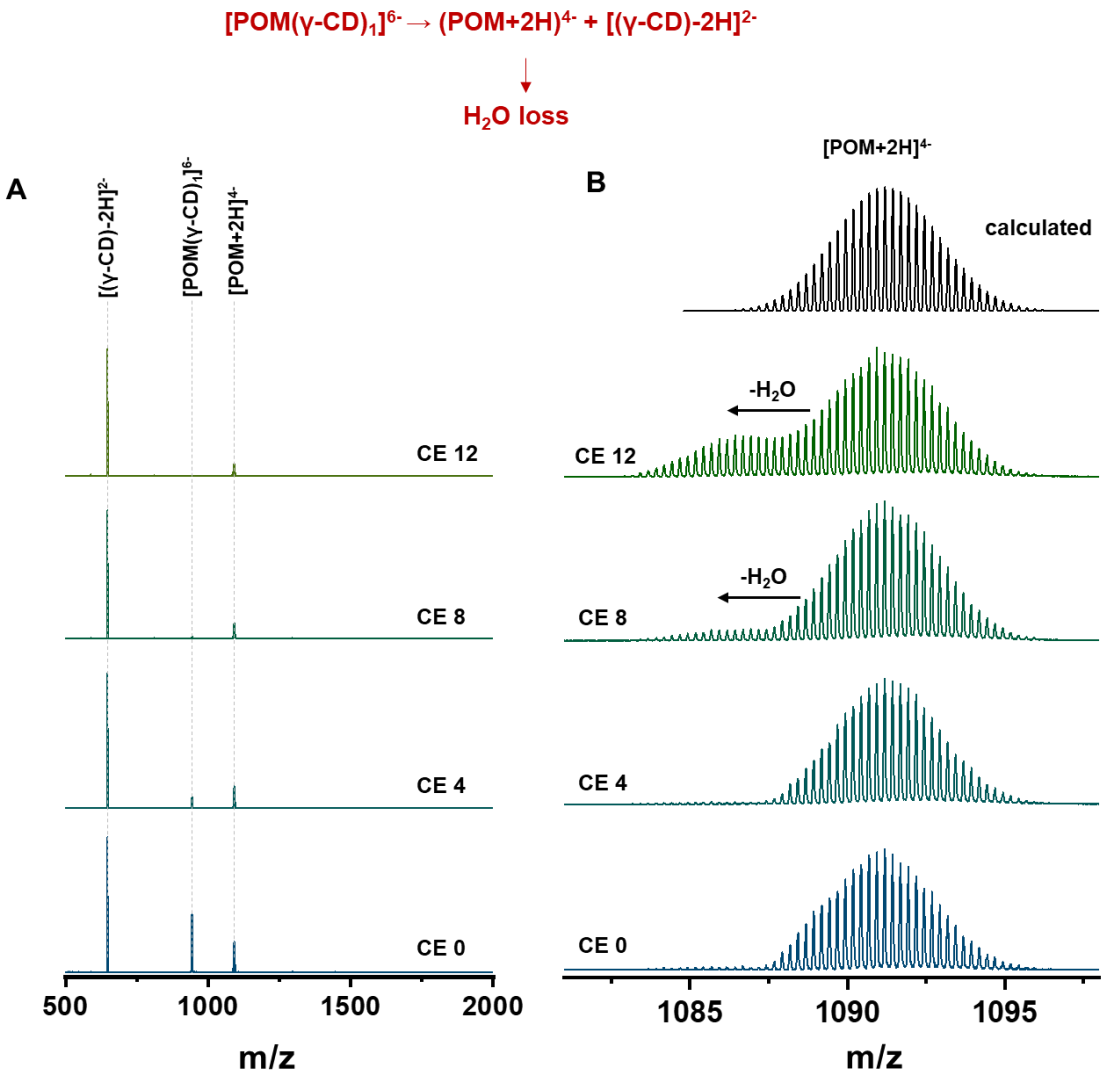

Fig. S8 A) CID of $[POM(\gamma\text{-}CD)_1]^{6-}$ at varying collision energies (CE) and B) expanded view in the m/z range ~1080-1098.

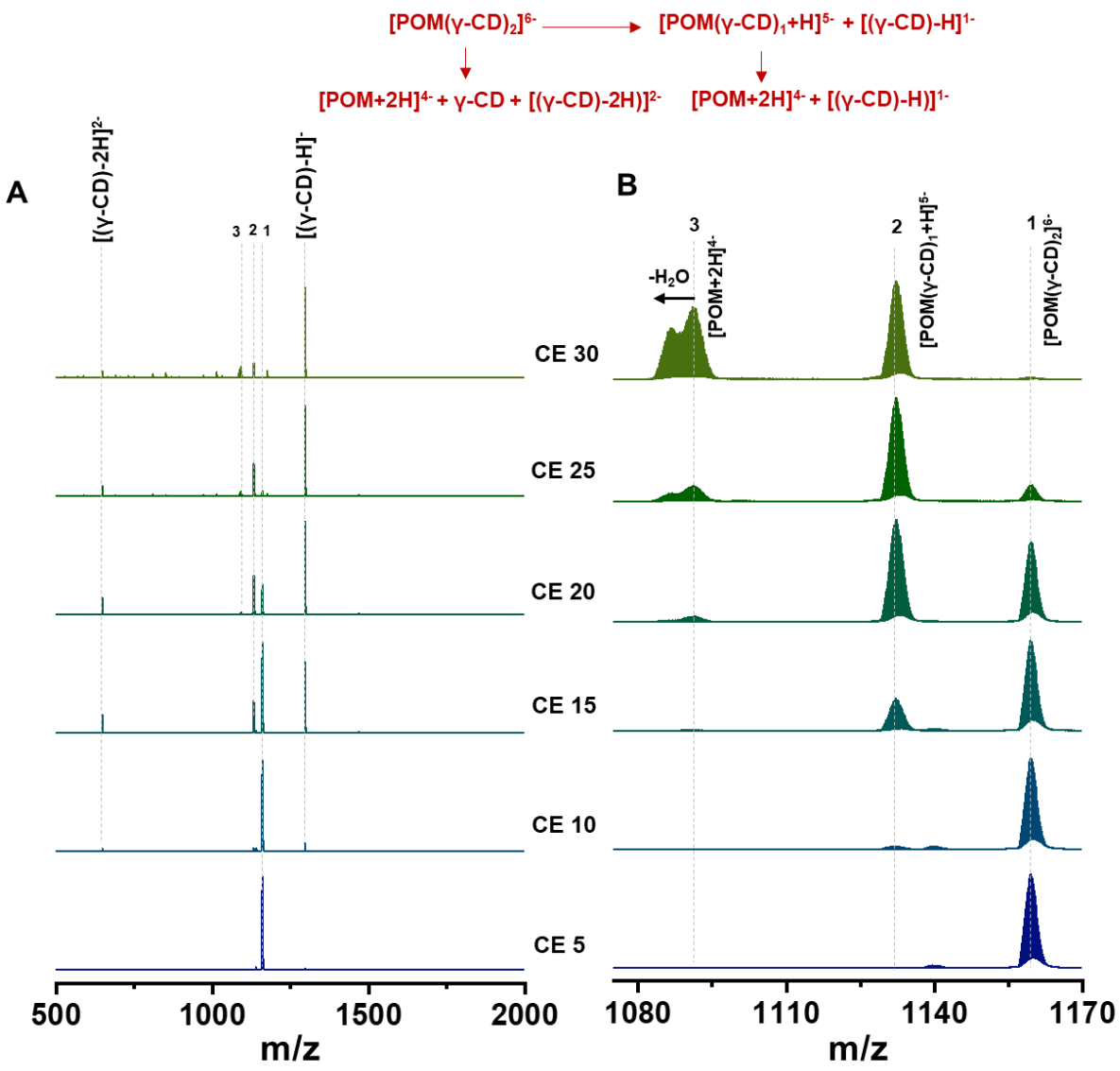

Fig. S9 A) CID of $[POM(\gamma\text{-}CD)_2]^{6-}$ at varying collision energies (CE) and B) expanded view in the m/z range ~1075-1170.

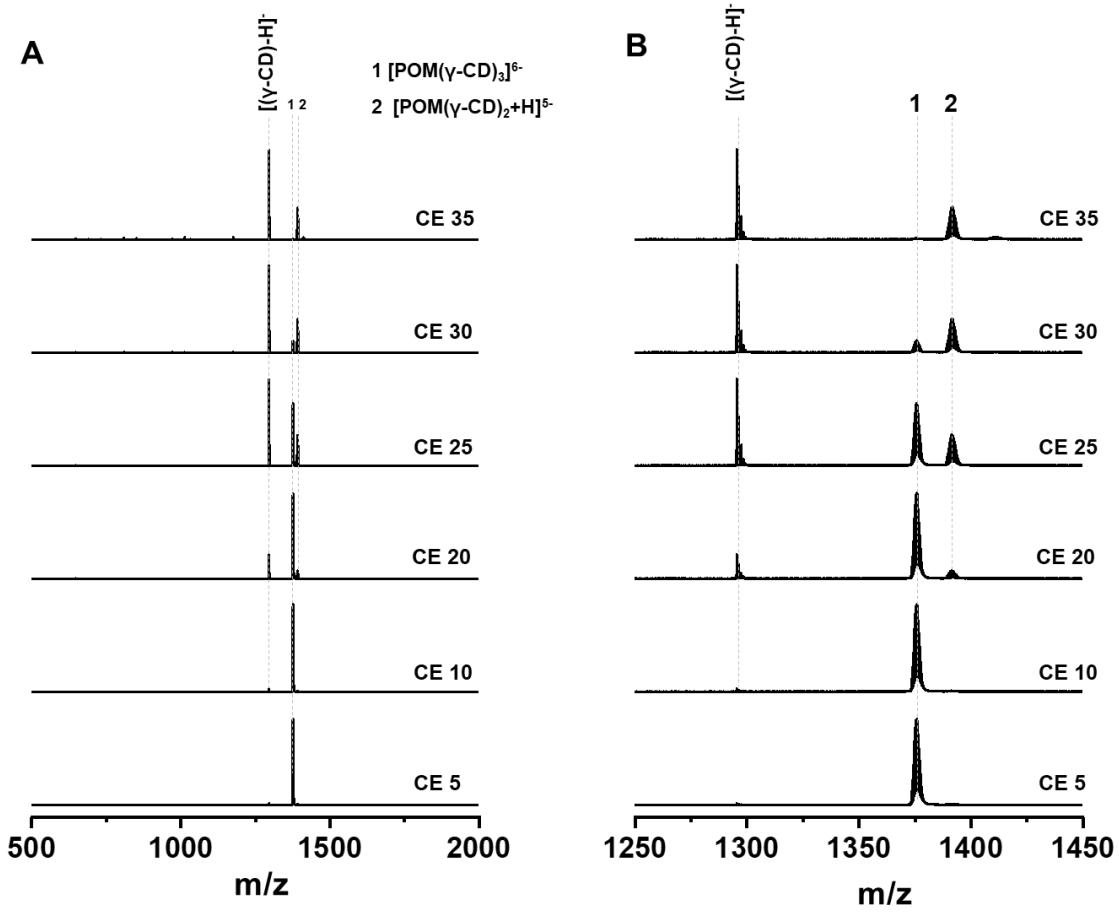

Fig. S10 A) CID of $[POM(\gamma\text{-}CD)_3]^{6-}$ at varying collision energies (CEs) and B) shows an expanded view in the m/z range 1250 to 1450.

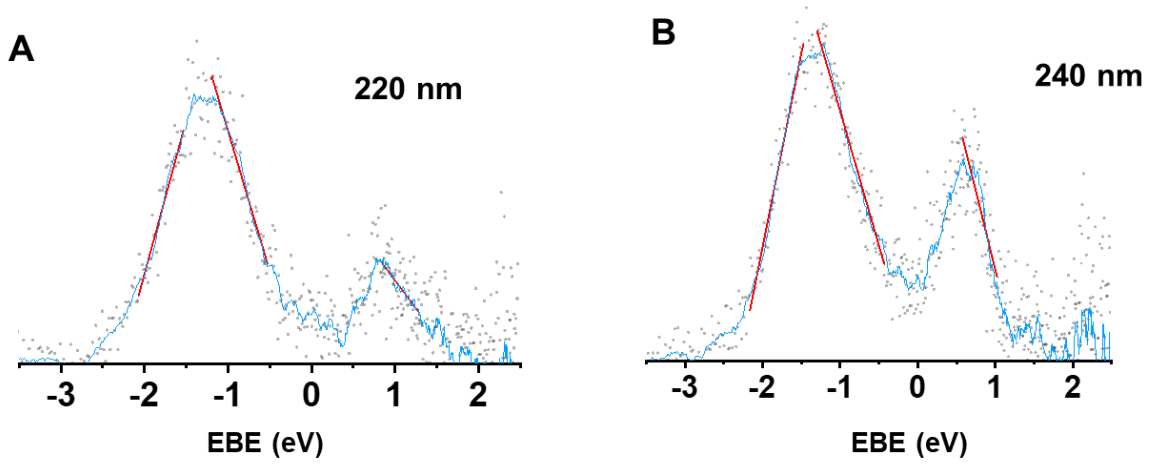

Fig. S11 Negative ion photoelectron spectra (PES) of $[KPOM]^{5-}$ measured at A) 220 nm and B) 240 nm.

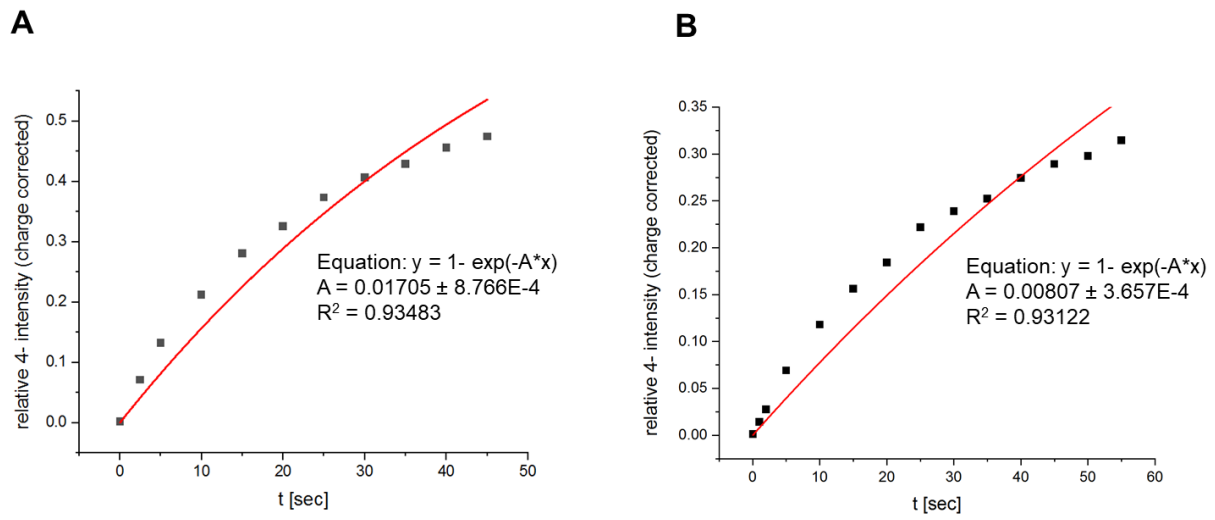

Fig. S12 Electron autodetachment from $[HPOM]^{5-}$ leading to the formation of $[HPOM]^{4-}$ in the ion-trap of the orbitrap instrument. The parent ion $[HPOM]^{5-}$ was electro-sprayed at capillary voltage of A) 120 °C and B) 30 °C, resulting in half-lives of ~40 s and ~85 s, respectively. The detachment rates strongly depend on the experimental conditions which affects the internal energy of the ions. Note that, a mono-exponential fit, according to first-order decay does not fit very well, probably because the ions are not in thermal equilibrium with the trap on the experimental timescale. That is, the "hotter" ions decay faster, thus cooling the ensemble. Details on this were not explored in the current study. However, given the negative VDEs determined in this study one would expect significant ground state electron tunneling autodetachment rates even at low vibrational temperatures.[3]

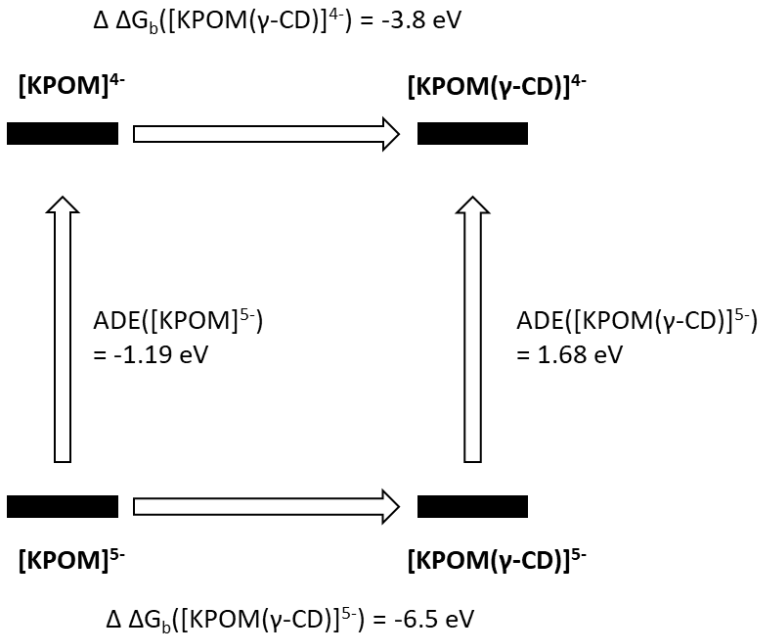

Fig. S13 Born-Haber cycle showing relation between ADE (adiabatic detachment energy) and $\Delta\Delta G_b$ (binding free energy).

Table S1. $^{TIMS}CCS_{N2}$ values of the observed species (mean values based on three different measurements and standard error of the mean)

Species	m/z	$^{TIMS}CCS_{N2}$ (Å^2)
$[HPOM]^{5-}$	873	515.4 ± 0.4
$[KPOM]^{5-}$	880	520.7 ± 0.5
$[K_2POM]^{4-}$	1110	445.9 ± 0.5
$[K_3POM]^{3-}$	1493	390.0 ± 0.3
$[POM(\gamma\text{-CD})_1]^{6-}$	943	665.0 ± 3.1
$[POM(\gamma\text{-CD})_2]^{6-}$	1159	728.6 ± 0.5 (i) 738.4 ± 0.4 (ii)
$[POM(\gamma\text{-CD})_3]^{6-}$	1376	790.6 ± 0.6 (i) 798.7 ± 0.6 (ii) 821.2 ± 0.6 (iii) 825.1 ± 0.5 (iv)
$[KPOM(\gamma\text{-CD})_1]^{5-}$	1139	593.9 ± 0.6 (i) 605.2 ± 1.0 (ii)
$[KPOM(\gamma\text{-CD})_2]^{5-}$	1399	683.3 ± 0.3 (i) 691.3 ± 0.5 (ii) 701.1 ± 0.7 (iii) 711.6 ± 0.5 (iv)
$[KPOM(\gamma\text{-CD})_3]^{5-}$	1658	755.1 ± 0.6 (i)

		763.9 ± 0.6 (ii) 784.7 ± 0.9 (iii) 792.3 ± 0.6 (iv)
$[K_2POM(\gamma\text{-CD})_1]^{4-}$	1434	543.2 ± 0.4 (i) 548.9 ± 0.6 (ii) 556.3 ± 0.7 (iii)
$[K_2POM(\gamma\text{-CD})_2]^{4-}$	1759	651.0 ± 0.6 (i) 657.7 ± 0.8 (ii) 662.8 ± 0.6 (iii)
$[K_2POM(\gamma\text{-CD})_3]^{4-}$	2083	712.0 ± 0.4 (i) 730.6 ± 0.4 (ii) 759.1 ± 0.4 (iii)

Table S2. Relative free energies (DFT) of the computed structures

Species	Relative free energy (ΔG) (eV)	Relative free energy (ΔG) (eV)
$[POM(\gamma\text{-CD})_1]^{6-}$	(r2SCAN-3c)	(ωB97X-V)
M1	0.00 eV	0.01
M2	0.01	0.00
M3	0.80	1.13
$[POM(\gamma\text{-CD})_2]^{6-}$	(r2SCAN-3c)	(ωB97X-V)
D1	0.43	-
D2	0.00	-

D3	0.20	-
$[KPOM(\gamma\text{-}CD)_1]^{5-}$	(r2SCAN-3c)	(ωB97X-V)
M'1	0.43	0.23
M'2	0.00	0.00
M'3	0.88	0.67
M'4	0.55	0.54

Table S3. Hydrogen bond (HB) analysis (using Jmol) of the calculated isomeric structures of $[POM(\gamma\text{-}CD)_1]^{6-}$. The number of bonds and the respective distances are analyzed.

	HBs between terminal O atoms of POM and ɤ-CD, HB distance (Å)	HBs between bridging O atoms of POM and ɤ-CD, HB distance (Å)	Intramolecular HBs in only CD, HB distance (Å)
M1	1.94 1.83 1.92 1.66 1.83 1.95 1.72 1.85	1.89 1.95 2.35	2.2 2.07 2.13 1.97
M2	1.79 1.78	2.38 2.4	1.96 1.82

	1.76 1.97 1.86 1.93 1.92 1.97 1.79 1.82 2.05 1.87 1.88		1.88 1.88 1.83 1.75 2.22 1.94
M3	2.08 1.94 1.85 1.93 1.86 1.86	2.47	2.08 2.07 2.18 2.17 2.24 2.17 2.07 2.17

References

1. Vonderach, M.; Ehrler, O. T.; Weis, P.; Kappes, M. M. *Anal. Chem.,*2011**, 83***,*1108-1115.
2. Wang, X.-B.; Wang, L.-S. *J. Chem. Phys.,*1999**, 111***,*4497-4509.
3. Arnold, K.; Balaban, T. S.; Blom, M. N.; Ehrler, O. T.; Gilb, S.; Hampe, O.; van Lier, J. E.; Weber, J. M.; Kappes, M. M. *J. Phys. Chem. A,*2003**, 107***,*794-803.